

Graphene/Au-Enhanced Plastic Clad Silica Fiber Optic Surface Plasmon Resonance Sensor

Wei Wei^{1,3} · Jinpeng Nong^{1,3} · Yong Zhu¹ · Guiwen Zhang¹ · Ning Wang¹ · Suqin Luo² · Na Chen¹ · Guilian Lan¹ · Chin-Jung Chuang^{3,4} · Yu Huang³

Received: 2 November 2016 / Accepted: 3 February 2017 / Published online: 24 February 2017
© Springer Science+Business Media New York 2017

Abstract Owing to its large surface-to-volume ratio and good biocompatibility, graphene has been identified as a highly promising candidate as the sensing layer for fiber optic sensors. In this paper, a graphene/Au-enhanced plastic clad silica (PCS) fiber optic surface plasmon resonance (SPR) sensor is presented. A sheet of graphene is employed as a sensing layer coated around the Au film on the PCS fiber surface. The PCS fiber is chosen to overcome the shortcomings of the structured microfibers and construct a more stable and reliable device. It is demonstrated that the introduction of graphene can enhance the intensity of the confined electric field surrounding the sensing layer, which results in a stronger light-matter interaction and thereby the improved sensitivity. The sensitivity of graphene-based fiber optic SPR sensor exhibits more than two times larger than that of the conventional gold film SPR fiber optic sensor. Furthermore, the dynamic response analyses reveal that the graphene/Au fiber optic SPR sensor exhibits a fast response (5 s response time) and excellent reusability

(3.5% fluctuation) to the protein biomolecules. Such a graphene/Au fiber optic SPR sensor with high sensitivity and fast response shows a great promise for the future biochemical application.

Keywords Fiber optic sensor · Surface plasmon resonance · Graphene · Plastic clad silica fiber

Introduction

Surface plasmon resonance (SPR)-based sensors [1–12] have been studied intensively for decades due to its label-free and real-time detection with high precision and sensitivity. In order to excite the SPR, the incident light reaching the metal/dielectric interface has to be modulated using a light propagation medium such as an optical prism [13, 14]. Typically, a plasmonic metal gold (Au) film is directly deposited onto the prism base to generate total internal reflection (TIR), which is very sensitive to the external sensing medium [15, 16]. A slight variation in the refractive index of the sensing medium gives rise to corresponding change in propagation constant of the SPR and, in turn, a large spectral shift in resonant dips. Then the refractive index change can be measured by detecting the spectral shifts of the resonant dip. Based on the similar sensing principle, coupling SPR to optical fiber technology has brought tremendous advancements by offering attractive advantages over the traditional prism-based SPR platforms, such as simplicity, cost effectiveness, and miniaturization [17–20]. Despite all these advantages, the fiber optic SPR setup still requires some improvements in order to reach the sensitivity of the traditional prism-based SPRs. To address this issue, different strategies have been employed by altering the surface morphology of the as-deposited plasmonic film [21], including the utilization of metal nanoparticles [22],

✉ Wei Wei
wwwei@cqu.edu.cn

✉ Yong Zhu
yongzhu@cqu.edu.cn

✉ Yu Huang
huangyu@cigit.ac.cn

¹ Key Laboratory of Optoelectronic Technology & Systems, Ministry of Education of China, College of Optoelectronic Engineering, Chongqing University, Chongqing 400044, China

² Chongqing Research Center for Advanced Materials, Chongqing Academy of Science and Technology, Chongqing 401123, China

³ Chongqing Institute of Green and Intelligent Technology, Chinese Academy of Sciences, Chongqing 401122, China

⁴ Department of Opto-Electronic Engineering, National Dong Hwa University, Hualien, Taiwan 97401, China

nanoholes [23], and nanodots [24]. These sub-wavelength-sized metallic nanostructures offer the unique effects of localized surface plasmon resonance (LSPR) with strong electromagnetic field confinement, resulting in the enhanced light-matter interaction and hence improved sensitivity. However, these methods remain complex, time consuming, and still very challenging for the precise control of the nanostructures. In addition, the metals cannot adsorb the molecules effectively due to the high surface inertness and intrinsic hydrophobicity [18], which limits the further improvement of sensitivity of fiber optic SPR sensor.

Graphene [25–27] composed of carbon atoms densely arrayed in a honeycomb crystal lattice has exhibited unique electronic and optical characteristics. It can efficiently adsorb a variety of polar molecules and biomolecules attributed to its large surface-to-volume ratio and the π -stacking interactions between graphene and biomolecules [28–31]. This excellent feature makes graphene a highly promising candidate as the sensing layer for fiber optic sensors. Recently, graphene has been applied to fiber optic sensing technology to construct various brand new sensors, such as graphene/tapered multimode evanescent wave absorption sensor [32], graphene-based D-shaped fiber multicore mode interferometer [33], and graphene-coated microfiber Bragg grating [34]. As for the fiber optic SPR sensor, there are several attempts to incorporate graphene as a sensing layer onto the surface of fiber but they only have theoretical consideration [35, 36]. Additionally, to our best knowledge, there are no experimental reports on the graphene/Au-enhanced fiber optic SPR sensor.

In this paper, a graphene/Au fiber optic SPR sensor is proposed using plastic clad silica (PCS) fiber. Graphene is introduced as a sensing layer attached on the Au surface coated on fiber core to enhance the sensitivity of graphene/Au fiber optic SPR sensor. Compared to traditional structured microfiber, PCS fiber possesses the advantages of easy manipulation, great illumination energy, and large diameter, which effectively avoids the shortcomings of structured microfiber such as fragile, unstable, and cross-sensitive. These features make it easier for PCS fiber to combine with graphene and construct a more stable and reliable device from the practical point of view. The performance of proposed sensor has been experimentally and theoretically investigated.

Materials and Methods

Reagents and Materials

Ethyl lactate, sulfuric acid, acetone, and glucose were purchased from Chongqing Chemical Group (China) and used without any further purification. Bovine serum albumin (BSA) was procured from Biosharp. Ultra-clean de-ionized water is obtained from a Milli-Q filtration system. Standard

glucose solutions with different concentrations were prepared in de-ionized water, and BSA solutions with different concentrations were prepared in saline solution. Multimode PCS optical fiber with numerical aperture (NA) of 0.37 and core diameter of 600 μm was purchased from Thorlabs. Au wire (99.99%) was purchased from a local supplier. All procedures were conducted at room temperature unless specified otherwise.

Preparation of Sensor Probe

The fabrication process of the proposed graphene/Au fiber optic SPR sensor is schematically demonstrated in Fig. 1. The optical fiber SPR probe was fabricated on the plastic optical fiber. As shown in Fig. 1a, the jacket and the cladding of 5 mm in length were removed mechanically from one end of the fiber. The unclad portion of the fiber was first cleaned with diluted sulfuric acid and then rinsed four to five times with de-ionized water and acetone. Cleaned unclad portion of the fiber was deposited with a thin gold film with thickness of 50 nm. The thickness of the depositing gold film on the fiber core can be controlled and monitored in real time, which is measured by quartz crystal monitor in-built in the thermal evaporation machine. The evaporation of gold was performed at 5×10^{-6} mbars. As the sensor is reflected type, the end face of fiber was also coated with gold film and used as a reflected mirror.

As shown in Fig. 1b, the large-area graphene monolayer was synthesized by chemical vapor deposition (CVD) method on a high-purity copper foil (No. 13439, Alfa Aesar), with flowing mixture of 3 sccm H_2 (70 mTorr) and 30 sccm CH_4 (340 mTorr) gases at 1000 °C. A layer of PMMA thin film was then coated on as-grow graphene on Cu foil as a transfer supporting layer by a spin coater. The graphene on the other side was removed by oxygen plasma processing. After completely removing Cu by the solution of FeCl_3 and HCl, the PMMA-supported floating graphene film was rinsed with de-ionized water twice and transferred onto the top of the sensor probe fixed on the SiO_2 substrate. It was then directly deposited around the gold surface of the sensor probe to form a graphene-coated sensor. Finally, the supporting polymer layers were removed by acetone treatment. The cross-section view of the fabricated graphene/Au fiber optic SPR sensor was shown in Fig. 1c.

The morphology of the proposed graphene/Au fiber optic SPR sensor was examined by field emission scanning electron microscopy (FESEM) and shown in Fig. 2a. The boundary of the graphene can be clearly seen without damage. To further confirm the existing of graphene on the Au-coated fiber surface, Raman spectra at region “A” was recorded via Raman spectrometer (Renishaw inVia Manual WiRE3.4) with 532-nm laser. The obtained Raman spectra in Fig. 2b clearly show two typical peaks of the graphene, including G-band

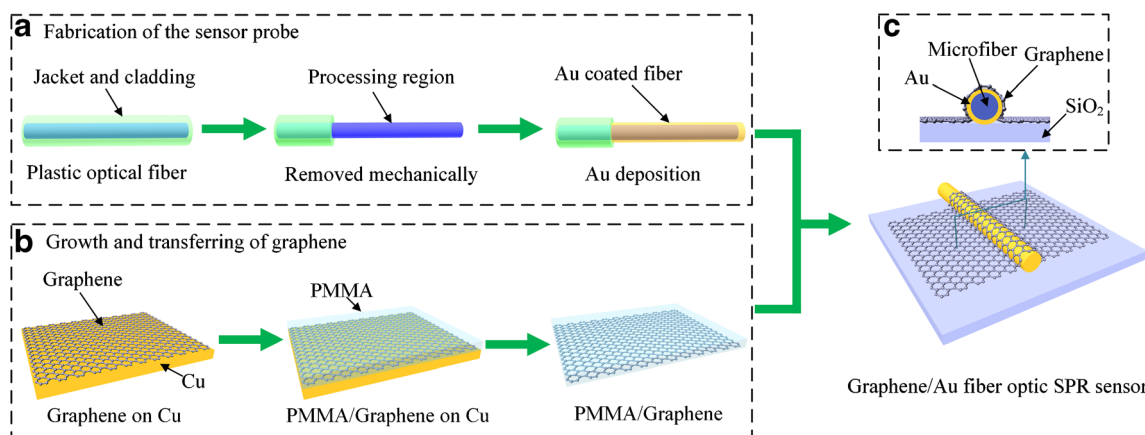


Fig. 1 Fabrication process of the proposed graphene/Au fiber optic SPR sensor. **a** Fabrication of the sensor probe. **b** Growth and transferring of graphene. **c** Cross-section view of the graphene/Au fiber optic SPR sensor

(1582 cm^{-1}) and 2D-band (2691 cm^{-1}). Both the symmetric 2D-band with a full width half maximum (FWHM) of 35 cm^{-1} and the high ratio of the peak intensities of 2D- to G-band (ratio ≈ 3) confirm the presence of a single-layer graphene [37]. In addition, the small D-band in this spectrum confirms the high quality of the graphene. Fig. 2c, d shows the intensity mapping of the G-band (light blue) and the 2D-band (yellow), respectively. These Raman mapping illustrate that the intensity distributions of the G- and 2D-band signals at the graphene surface are clearly distinguished from those at the Au surface, further demonstrating the presence of the high quality large-area graphene on fiber surface.

Experimental Setup

The schematic diagram of the measurement system using SPR-based fiber optic sensor is shown in Fig. 3a. One end of the sensor was connected to the end of a 2×1 fiber coupler and the other end with the sensing area was immersed into the target solution. The white light emitted from a tungsten-halogen light source (Avalight-HAL, Avantes) was conducted into the sensor through the 2×1 fiber coupler. When the wave vector of the incident light matches that of surface plasmon, SPR wave can be resonantly excited. Within the Au/fiber interface, graphene enhanced the interaction between the SPR

Fig. 2 **a** SEM image of monolayer graphene on Au-coated fiber. **b** Raman spectroscopy of region A denoted in **a**. Raman intensity mapping of **c** G-band (1582 cm^{-1}) and **d** 2D-band (2691 cm^{-1})

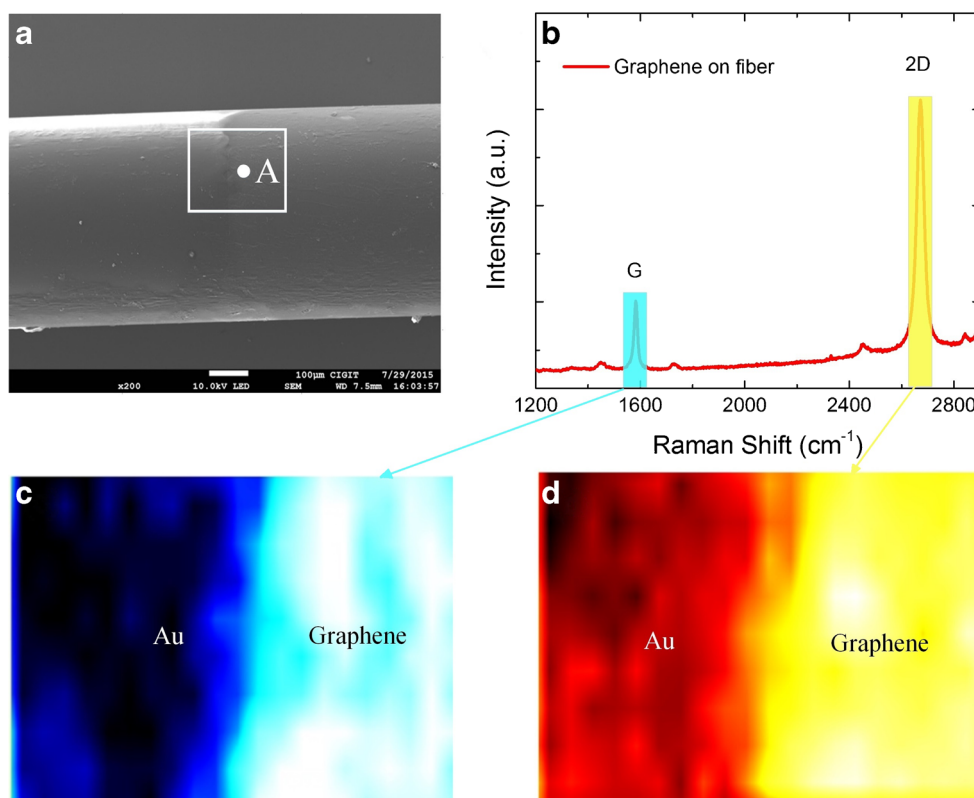
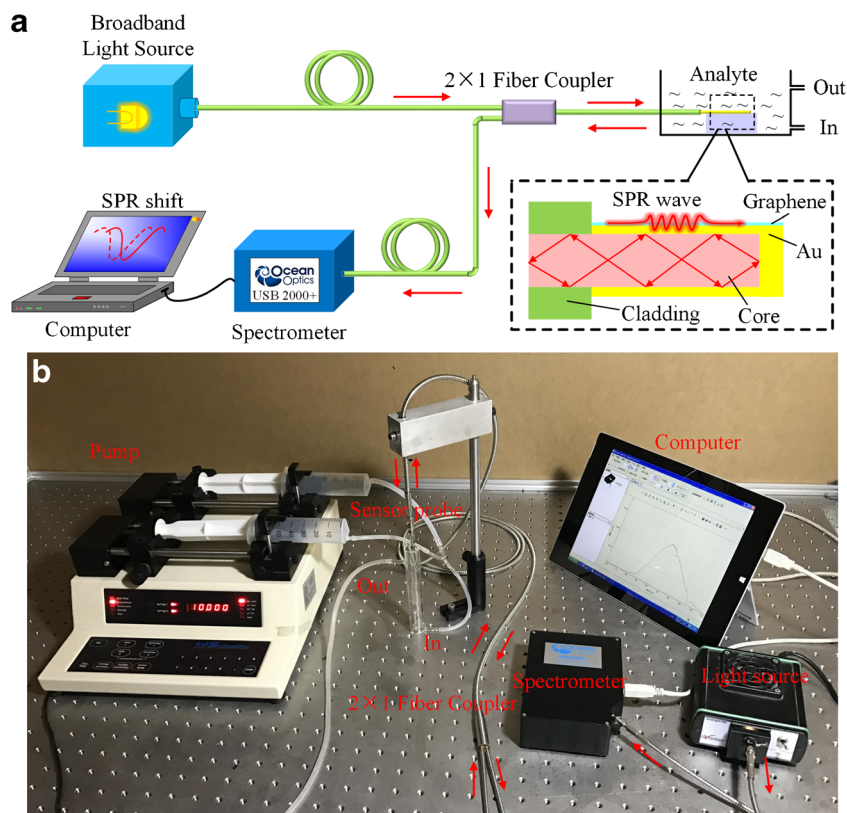


Fig. 3 **a** Schematic of graphene/Au fiber optic SPR sensing system. **b** The photo of the experimental setup



wave and the analyte. When the target molecules were adsorbed by the graphene, the permittivity of the graphene is changed, which induced the variation of the refractive index on the sensing region. Such that the SPR spectrum shifts could be measured according to the refractive index variation, and the concentration changes could be detected. The SPR spectrum shifts of the graphene/Au layer-coated sensor were captured by a fiber optic spectrometer (USB2000+, Ocean Optics), which was connected to the other end of the 2×1 fiber coupler. The resonance spectra were recorded and analyzed by a program written in C++ and Matlab. The corresponding photo of the experimental setup is shown in Fig. 3b.

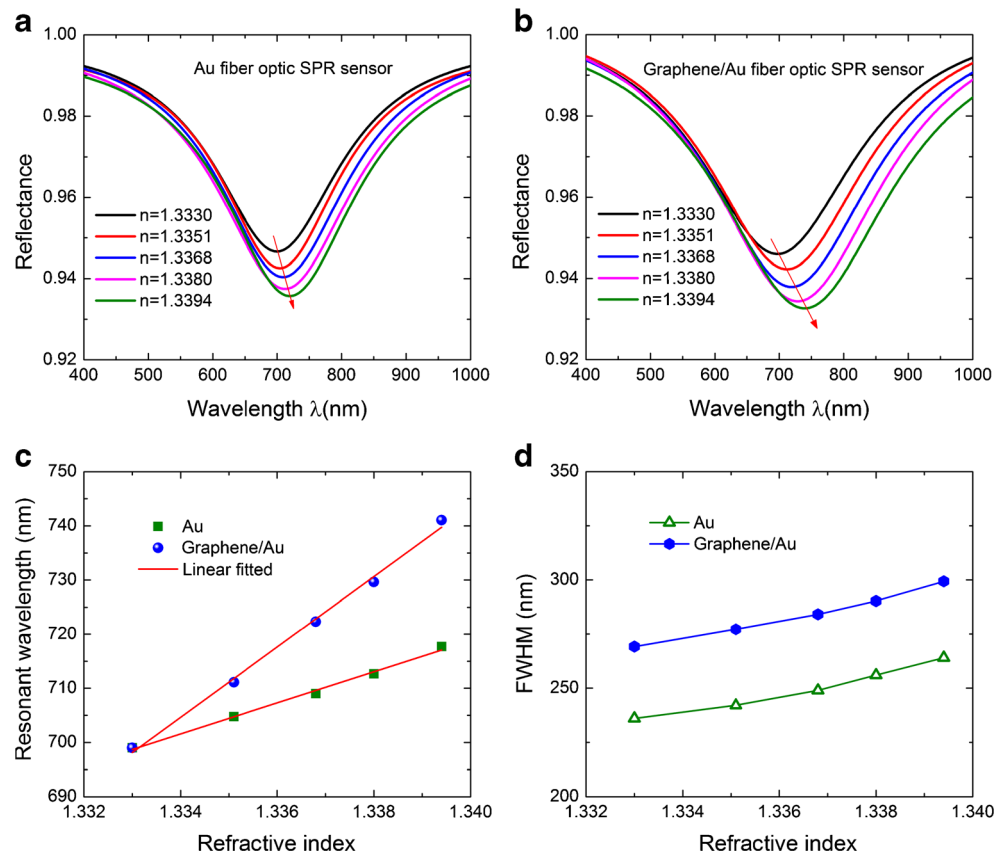
Results and Discussion

We first study the sensing characteristic of this graphene/Au fiber optic SPR sensor to its surrounding environment. The sensor probes were immersed in the standard glucose solutions with refractive index ranging from 1.333 to 1.3394 refractive index units (RIU). The reflection spectra of the fiber optic SPR sensor without graphene coating layer are shown in Fig. 4a. Obvious resonant dips originating from the excitation of SPR wave at the Au/fiber interface can be observed. The resonant wavelength redshifts from 698.8 to 717.7 nm as the refractive index of the glucose solution increases from 1.333 to 1.3394. In the case of the graphene existence, the reflection

spectra are provided in Fig. 4b. The original position of resonant wavelength of the graphene/Au fiber optic SPR sensor is slightly larger than that of the sensor without graphene, which is attributed to the large real part of the dielectric function of graphene layer. Moreover, the graphene/Au fiber optic SPR sensor exhibits a larger redshift (41.6 nm) of resonant wavelength from 699.5 to 741.1 nm compared to that (18.9 nm) of the sensor without graphene. These results indicate that the present of graphene can improve the sensing performance of fiber optic SPR sensor.

To quantitatively evaluate the performance of the fiber optic SPR sensor, the resonant wavelengths of the fiber optic SPR sensors with and without graphene as a function of refractive index are extracted from Fig. 4a, b, respectively, and the data are plotted and could be fitted linearly as shown in Fig. 4c, d. The approximately linear relationships between the SPR resonant wavelength and the refractive index ranges of 1.333 to 1.3394 can be observed with high linear coefficient of 0.9935 and 0.9947, respectively. The refractive index sensitivity is defined as $S_n = \delta\lambda_{\text{res}}/\delta n_s$, where δn_s is the change in the refractive index of the solution and $\delta\lambda_{\text{res}}$ is the shift in the corresponding resonant wavelength. Compared to the sensor coated only with gold film exhibiting 2869 nm/RIU in the range of 1.333 to 1.3394, the refractive index sensitivity of sensor with graphene/Au hybrid structure has been improved to 6500 nm/RIU in the identical refractive index range. The graphene/Au fiber optic SPR sensor exhibited approximate

Fig. 4 **a** Reflection spectra of Au fiber optic SPR sensor with varying refractive index of glucose solution. **b** Reflection spectra of graphene/Au fiber optic SPR sensor with varying refractive index of glucose solution. The SPR peak spectra in **a** and **b** were obtained by data analysis with Lorentzian fitting [38]. **c** The relationship between the resonant wavelength of two kinds of fiber optic SPR sensors and the refractive index of solution. The lines are linearly fitted. **d** The relationship between FWHM and the refractive index of solution



2.27-fold-improved sensitivity compared to the traditional fiber optic SPR sensor without graphene layer.

The figure of merit (FOM) defined as $FOM = S_r/FWHM$ is used to comprehensively characterize the performance of SPR sensor. FWHM is the full width at half minimum of the resonance spectrum and defined as the corresponded wavelength width at the half percentage of the normalized resonant dip. The FWHM of two kinds of fiber optic SPR sensors are extracted from Fig. 4a, b, respectively, and plotted in Fig. 4d. One can see that the FWHM of the graphene/Au fiber optic SPR sensor is slightly larger than that of the sensor without graphene. This reason is attributed to the fact that graphene is a lossy dielectric having complex dielectric constant. Hence, the damping associated with the SPR wave in the graphene region results in the broadening of reflection curve [39]. Although the presence of graphene could broaden the FWHM, the averaged FOM of the graphene/Au fiber optic SPR sensor is calculated to be 22.8 RIU^{-1} , which is approximately two times larger than that (11.5 RIU^{-1}) of the Au fiber optic SPR sensor.

The calibrated fiber optic SPR sensors were further utilized to evaluate the concentration of protein biomolecules. A series of BSA solutions with different concentrations C ranging between 0 and 2 mg/ml were prepared as the target analytes. The evolution of reflection spectra recorded from the fiber optic SPR sensor is shown in Fig. 5a. The resonant wavelength

exhibits a redshift of 6.1 nm in response to the increasing concentration of BSA solution from 0 to 2 mg/ml. As expected, the presence of graphene can enhance the sensitivity of the fiber optic SPR sensor, as shown in Fig. 5b. The fiber optic SPR sensor coated with graphene exhibits a 13.8-nm redshift by the same amount of change in concentration of BSA solvent. The resonant wavelengths of the two kinds of sensors as function of BSA concentration are further extracted and compared in Fig. 5c. The fitted lines of the extracted resonant wavelengths have large linear coefficients of 0.9973 and 0.9925, respectively. The sensitivity of the fiber optic SPR sensors with graphene/Au hybrid structure is estimated to be $7.01 \text{ nm}/(\text{mg}/\text{ml})$, which is 2.35 times larger than that of the sensor only coated with Au ($2.98 \text{ nm}/(\text{mg}/\text{ml})$). In addition, FWHM of two kinds of fiber optic SPR sensors is shown in Fig. 5d, and the FOM of the graphene/Au fiber optic SPR sensor exhibited approximate 2.18 times larger than that of the sensor without graphene layer, also indicating the improvement of overall performance by the present of graphene.

To evaluate the response time of graphene/Au fiber optic SPR sensor, the solutions were switched between saline solution and BSA solution. Fig. 6a shows the resonant wavelength as a function of time when the flowing solvent was switched from saline solution to 1.0 mg/ml BSA solution. Due to the pumping of 1.0 mg/ml BSA solution, the resonant wavelength gradually increases from 713.2 to 721.3 nm and reaches a

Fig. 5 **a** Reflection spectra of Au fiber optic SPR sensor with varying concentration of BSA solution. **b** Reflection spectra of graphene/Au fiber optic SPR sensor with varying concentration of BSA solution. **c** The relationship between the resonant wavelength of two kinds of fiber optic SPR sensors and the concentration of solution. The lines are linearly fitted. **d** The relationship between FWHM and the concentration of solution

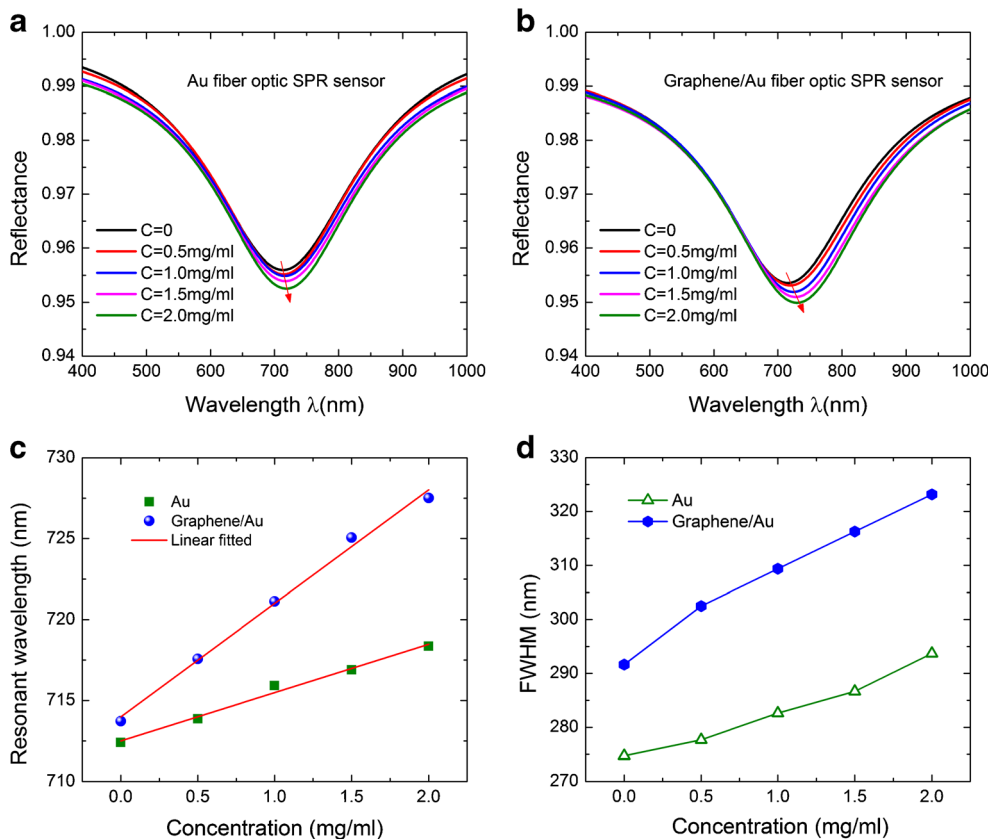


Fig. 6 Dynamic response of sensor to the flowing solvent. **a** The resonant wavelength of graphene/Au fiber optic SPR sensor as a function of time when the solvent was switched from saline solution to 1.0 mg/ml BSA solution. The signal was recorded every second. **b** The resonant wavelength when solvent was switched between saline solution and 1.0 mg/ml BSA solution. The signal was recorded every 5 s. **c** The resonant wavelength of the sensor as a function of time when the solvent was switched between saline solution and different concentrations of BSA solution. The signal was recorded every 10 s

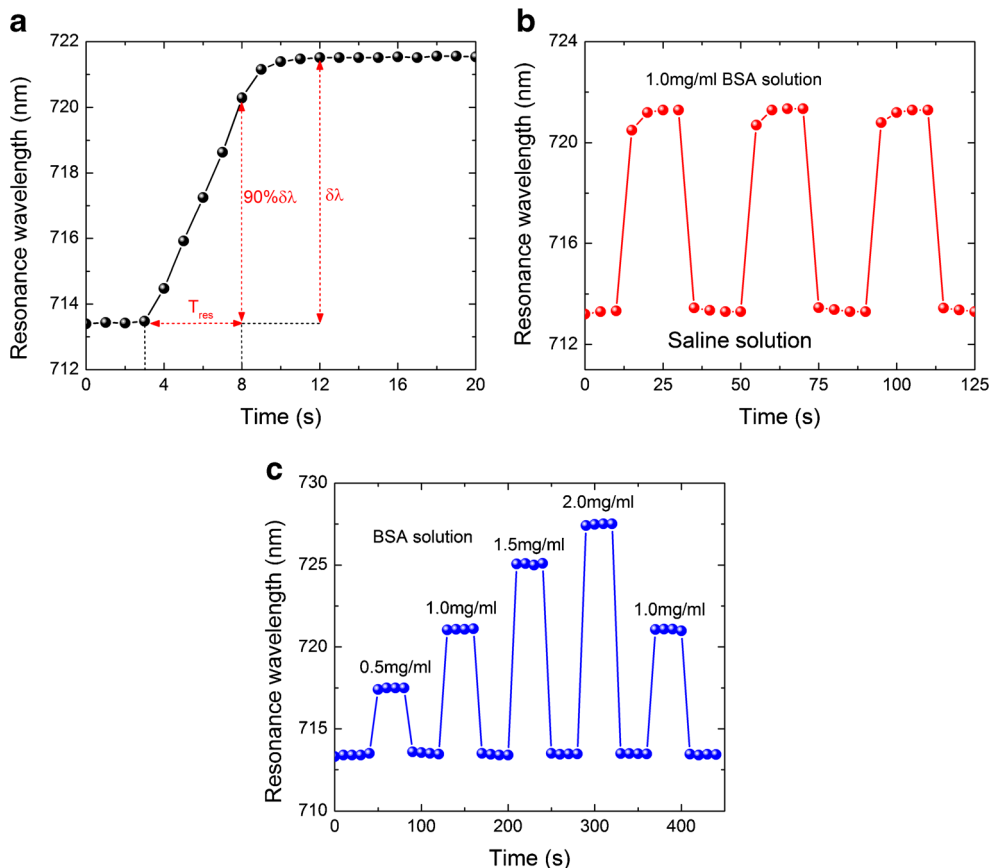
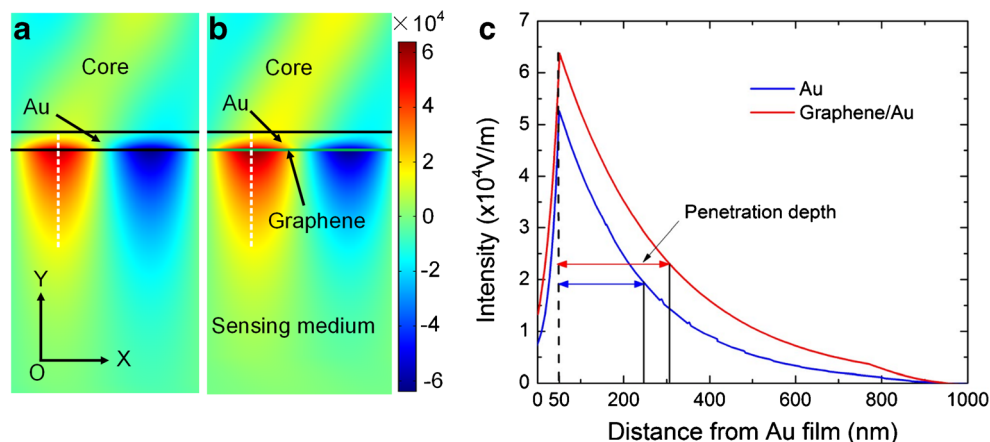


Fig. 7 FEA simulation of resonant graphene/Au sensing film. Electric field distribution of Au fiber optic SPR sensor (a) and graphene/Au fiber optic SPR sensor (b) at the resonant wavelength. c Cross-section plot of the total electric field exponentially decaying along the direction perpendicular to the graphene/Au sensing layer



stable value. The response time (T_{res} , defined as the time required for a sensor to reach 90% of signal change $\delta\lambda$) of the sensor was measured to be 5 s. Such a response time is much shorter than that of the graphene-covered fiber optic sensors [33, 34] and the traditional fiber optic SPR sensor [22], indicating the fast response of the graphene/Au fiber optic SPR sensor.

The reproducibility of the graphene/Au fiber optic SPR sensor was also investigated. The dynamic response of the sensor to the change of flowing solvent switched between saline solution and 1.0 mg/ml BSA solution is provided in Fig. 6b. Three replicate cycles of this pumping sequence were performed. It is observed that the resonant wavelength changes between ~ 713.2 and ~ 721.3 nm, and the relative standard deviation of resonant wavelength perturbed by the presence of saline solution and 1.0 mg/ml BSA solution is calculated to be 2.3 and 4.1%, respectively, which demonstrates the good reproducibility of the proposed graphene/Au fiber optic SPR sensor. Fig. 6c shows the dynamic response of resonant wavelength to a successive pumping of a mixture with different concentrations of BSA solution. The resonant wavelength was stepped up and down with the pumping of four mixtures. The final injection of saline solution makes the resonant wavelength go back to its initial position with negligible hysteresis. Meanwhile, fluctuation of the resonant wavelength recorded at saline solution after several pumping cycles is only 3.5%, indicating the acceptable reusability of this sensor.

Finally, finite element analysis (FEA) method is introduced employing COMSOL Multiphysics to explain the enhanced sensing performance by the present of monolayer graphene. The fiber is simplified using 2D model since the resonant wavelength is much smaller than the core diameter of PCS optical fiber ($\sim 1/860$). In the model, the dielectric constant of Au (50 nm) comes from handbook of Palik [40], the refractive index of fiber core is 1.45, and the surface conductivity of graphene is modeled as $\sigma_0 = e^2/4\hbar$ in the considering visible region [41], where e is the elementary charge and \hbar is the reduced Planck's constant. Periodic boundary condition is applied along the X-direction, while in the propagation direction,

scattering boundary conditions and perfectly matched layers are applied at the two ends of computational space. Within the incident angle range (larger than 79.8°) allowed by the numerical aperture (0.37) of the fiber, the light can couple into and propagate in the fiber. Our results show the SPR mode is resonantly excited at Au/fiber interface at incident angle of 82.8° , which is indeed in the allowed angle range of propagating in the fiber. The calculated electric field mode profiles of Au fiber optic SPR sensor and graphene/Au fiber optic SPR sensor are displayed and compared in Fig. 7a, b, respectively. One can see that the highly confined electric field of the two structures exhibit the similar distribution profiles at the sensing medium/Au interface, which significantly enhances the light-matter interaction. Meanwhile, the present of the graphene can enhance the confined electric field with maximum intensity of 6.4×10^4 V/m (Fig. 7b). To further quantitatively illustrate the penetration characteristic of the electric field, the electric field intensity of the two structures along the Y-direction (white dashed line) that is perpendicular to sensing interface is extracted from Fig. 7a, b, and compared in Fig. 7c. It is observed that the electric field generated by graphene/Au hybrid structure is stronger than that of the structure without graphene and the electric field exponentially decays into the sensing medium. The penetration depth is defined as the distance where the electric field intensity decreased to be $1/e$. For the graphene/Au structure, the penetration depth of the electric field into the sensing medium is 256 nm, which is larger than that (195 nm) of the structures without monolayer graphene. Thus, the introduction of graphene sensing layer can enhance the intensity of the electric field surrounding the sensing layer and enables the sensor to be more sensitive to the change of medium.

Conclusions

In this work, a fiber optic SPR sensor with graphene/Au hybrid structure has been proposed and theoretically and experimentally analyzed. The introduction of graphene sensing

layer on the gold surface can greatly enhance the sensitivity of the fiber optic SPR sensor. The proposed sensor experiences a larger redshift of resonant wavelength compared to the conventional gold film fiber optic SPR sensor, which shows that the proposed sensor exhibits enhanced sensitivity. The repeatable dynamic response of resonant wavelength in response to the flowing solvent indicates the stability of this proposed sensor and shows its potential in the future chemical and biological application.

Acknowledgements This work is supported by the National Natural Science Foundation of China (Grant No. 61405021, 61675037), National High Technology Research and Development Program of China (Grant No. 2015AA034801), Natural Science Foundation of Chongqing, China (Grant No. cstc2014jcyjA40045), and Visiting Scholar Foundation of Key Laboratory of Optoelectronic Technology & Systems (Chongqing University), Ministry of Education.

References

- Singh P (2016) SPR biosensors: historical perspectives and current challenges. *Sensor Actuat B- Chem* 229:110–130. doi:10.1016/j.snb.2016.01.118
- Zhang D, Lu Y, Jiang J, Zhang Q, Yao Y, Wang P, Chen B, Cheng Q, Liu GL, Liu Q (2015) Nanoplasmonic biosensor: coupling electrochemistry to localized surface plasmon resonance spectroscopy on nanocup arrays. *Biosens Bioelectron* 67:237–242. doi:10.1016/j.bios.2014.08.022
- Mohseni S, Moghadam TT, Dabirmanesh B, Jabbari S, Khajeh K (2016) Development of a label-free SPR sensor for detection of matrix metalloproteinase-9 by antibody immobilization on carboxymethyl dextran chip. *Biosens Bioelectron* 81:510–516. doi:10.1016/j.bios.2016.03.038
- Barrios CA, Canalejas-Tejero V, Herranz S, Urraca J, Moreno-Bondi MC, Avella-Oliver M, Maquieira A, Puchades R (2015) Aluminum nanoholes for optical biosensing. *Biosensors* 5(3): 417–431. doi:10.3390/bios5030417
- Liu Q, Tu X, Kim KW, Kee JS, Shin Y, Han K, Yoon Y-J, Lo G-Q, Park MK (2013) Highly sensitive Mach–Zehnder interferometer biosensor based on silicon nitride slot waveguide. *Sensor Actuat B- Chem* 188:681–688. doi:10.1016/j.snb.2013.07.053
- Cai D, Lu Y, Lin K, Wang P, Ming H (2008) Improving the sensitivity of SPR sensors based on gratings by double-dips method (DDM). *Opt Express* 16(19):14597–14602. doi:10.1364/OE.16.014597
- Tokel O, Yildiz UH, Inci F, Dumus NG, Ekiz OO, Turker B, Cetin C, Rao S, Sridhar K, Natarajan N, Shafiee H, Dana A, Demirci U (2015) Portable microfluidic integrated plasmonic platform for pathogen detection. *Sci Rep* 5:9152. doi:10.1038/srep09152
- Yin LL, Wang SP, Shan XN, Zhang ST, Tao NJ (2015) Quantification of protein interaction kinetics in a micro droplet. *Rev Sci Instrum* 86(11):114101. doi:10.1063/1.4934802
- Zhou B, Xiao X, Liu T, Gao Y, Huang Y, Wen W (2016) Real-time concentration monitoring in microfluidic system via plasmonic nanocrescent arrays. *Biosens Bioelectron* 77:385–392. doi:10.1016/j.bios.2015.09.054
- Liang J, Yao C, Li X, Wu Z, Huang C, Fu Q, Lan C, Cao D, Tang Y (2015) Silver nanoprisms etching-based plasmonic ELISA for the high sensitive detection of prostate-specific antigen. *Biosens Bioelectron* 69:128–134. doi:10.1016/j.bios.2015.02.026
- Lin K, Lu Y, Chen J, Zheng R, Wang P, Ming H (2008) Surface plasmon resonance hydrogen sensor based on metallic grating with high sensitivity. *Opt Express* 16(23):18599–18604. doi:10.1364/OE.16.018599
- Yu H, Xiong L, Chen Z, Li Q, Yi X, Ding Y, Wang F, Lv H, Ding Y (2014) Ultracompact and high sensitive refractive index sensor based on Mach–Zehnder interferometer. *Opt Lasers Eng* 56:50–53. doi:10.1016/j.optlaseng.2013.12.006
- Maurya JB, Prajapati YK, Singh V, Saini JP (2015) Sensitivity enhancement of surface plasmon resonance sensor based on graphene–MoS₂ hybrid structure with TiO₂–SiO₂ composite layer. *Appl Phys A Mater Sci Process* 121(2):525–533. doi:10.1007/s00339-015-9442-3
- Zeng S, Hu S, Xia J, Anderson T, Dinh X-Q, Meng X-M, Coquet P, Yong K-T (2015) Graphene–MoS₂ hybrid nanostructures enhanced surface plasmon resonance biosensors. *Sensor Actuat B- Chem* 207:801–810. doi:10.1016/j.snb.2014.10.124
- Gupta BD, Verma RK (2009) Surface plasmon resonance-based fiber optic sensors: principle, probe designs, and some applications. *J Sensors* 2009:1–12. doi:10.1155/2009/979761
- Tabassum R, Gupta BD (2016) SPR based fiber-optic sensor with enhanced electric field intensity and figure of merit using different single and bimetallic configurations. *Opt Commun* 367:23–34. doi:10.1016/j.optcom.2016.01.014
- Caucheteur C, Guo T, Albert J (2015) Review of plasmonic fiber optic biochemical sensors: improving the limit of detection. *Anal Bioanal Chem* 407(14):3883–3897. doi:10.1007/s00216-014-8411-6
- Arghir I, Spasic D, Verlinden BE, Delpont F, Lammertyn J (2015) Improved surface plasmon resonance biosensing using silanized optical fibers. *Sensor Actuat B- Chem* 216:518–526. doi:10.1016/j.snb.2015.04.069
- Zhao J, Cao S, Liao C, Wang Y, Wang G, Xu X, Fu C, Xu G, Lian J, Wang Y (2016) Surface plasmon resonance refractive sensor based on silver-coated side-polished fiber. *Sensor Actuat B- Chem* 230: 206–211. doi:10.1016/j.snb.2016.02.020
- Huang Y, Wu D, Chuang C-J, Nie B, Cui H, Yun W (2015) Theoretical analysis of tapered fiber optic surface plasmon resonance sensor for voltage sensitivity. *Opt Fiber Technol* 22:42–45. doi:10.1016/j.yofte.2015.01.004
- Arghir I, Delpont F, Spasic D, Lammertyn J (2015) Smart design of fiber optic surfaces for improved plasmonic biosensing. *New Biotechnol* 32(5):473–484. doi:10.1016/j.nbt.2015.03.012
- Rithesh Raj D, Prasanth S, Vineeshkumar TV, Sudarsanakumar C (2016) Surface plasmon resonance based fiber optic dopamine sensor using green synthesized silver nanoparticles. *Sensor Actuat B- Chem* 224:600–606. doi:10.1016/j.snb.2015.10.106
- Dhawan A, Gerhold MD, Muth JF (2008) Plasmonic structures based on subwavelength apertures for chemical and biological sensing applications. *IEEE Sensors J* 8(6):942–950. doi:10.1109/JSEN.2008.923933
- Lin Y, Zou Y, Mo Y, Guo J, Lindquist RG (2010) E-beam patterned gold nanodot arrays on optical fiber tips for localized surface plasmon resonance biochemical sensing. *Sensors* 10(10):9397–9406. doi:10.3390/s101009397
- Novoselov KS, Fal'ko VI, Colombo L, Gellert PR, Schwab MG, Kim K (2012) A roadmap for graphene. *Nature* 490(7419):192–200. doi:10.1038/nature11458
- Li Y, Yan H, Farmer DB, Meng X, Zhu W, Osgood RM, Heinz TF, Avouris P (2014) Graphene plasmon enhanced vibrational sensing of surface-adsorbed layers. *Nano Lett* 14(3):1573–1577. doi:10.1021/nl404824w
- Wei W, Nong J, Tang L, Zhu Y, Shi H (2016) Coupling of graphene plasmonics modes induced by near-field perturbation at terahertz frequencies. *Plasmonics* 11(4):1109–1118. doi:10.1007/s11468-015-0149-2

28. Rodrigo D, Limaj O, Janner D, Etezadi D, Abajo FJGD, Pruneri V, Altug H (2015) Mid-infrared plasmonic biosensing with graphene. *Science* 349(6244):165–168. doi:[10.1126/science.aab2051](https://doi.org/10.1126/science.aab2051)
29. Wei W, Nong J, Tang L, Zhang G, Yang J, Luo W (2016) Conformal graphene-decorated nanofluidic sensors based on surface plasmons at infrared frequencies. *Sensors* 16(6):899. doi: [10.3390/s16060899](https://doi.org/10.3390/s16060899)
30. Salihoglu O, Balci S, Kocabas C (2012) Plasmon-polaritons on graphene-metal surface and their use in biosensors. *Appl Phys Lett* 100(21):213110. doi:[10.1063/1.4721453](https://doi.org/10.1063/1.4721453)
31. Reckinger N, Vlad A, Melinte S, Colomer J-Fo, Sarrazin MI (2013) Graphene-coated holey metal films: tunable molecular sensing by surface plasmon resonance. *Appl Phys Lett* 102:211108. doi: [10.1063/1.4808095](https://doi.org/10.1063/1.4808095)
32. Qiu H, Gao S, Chen P, Li Z, Liu X, Zhang C, Xu Y, Jiang S, Yang C, Huo Y, Yue W (2016) Evanescent wave absorption sensor based on tapered multimode fiber coated with monolayer graphene film. *Opt Commun* 366:275–281. doi:[10.1016/j.optcom.2015.12.071](https://doi.org/10.1016/j.optcom.2015.12.071)
33. Wu Y, Yao BC, Zhang AQ, Cao XL, Wang ZG, Rao YJ, Gong Y, Zhang W, Chen YF, Chiang KS (2014) Graphene-based D-shaped fiber multicore mode interferometer for chemical gas sensing. *Opt Lett* 39(20):6030–6033. doi:[10.1364/OL.39.006030](https://doi.org/10.1364/OL.39.006030)
34. Wu Y, Yao B, Zhang A, Rao Y, Wang Z, Cheng Y, Gong Y, Zhang W, Chen Y, Chiang KS (2014) Graphene-coated microfiber Bragg grating for high-sensitivity gas sensing. *Opt Lett* 39(5):1235–1237. doi:[10.1364/OL.39.001235](https://doi.org/10.1364/OL.39.001235)
35. Feng D, Liu G, Zhang M, Jia D (2013) D-shaped fiber optic SPR biosensors based on a metal-graphene structure. *Chin Opt Lett* 11(11):110607. doi:[10.3788/COL201311.110607](https://doi.org/10.3788/COL201311.110607)
36. Fu H, Zhang S, Chen H, Weng J (2015) Graphene enhances the sensitivity of fiber-optic surface plasmon resonance biosensor. *IEEE Sensors J* 15(10):5478–5482. doi:[10.1109/JSEN.2015.2442276](https://doi.org/10.1109/JSEN.2015.2442276)
37. Kim SJ, Choi T, Lee B, Lee S, Choi K, Park JB, Yoo JM, Choi YS, Ryu J, Kim P, Hone J, Hong BH (2015) Ultraclean patterned transfer of single-layer graphene by recyclable pressure sensitive adhesive films. *Nano Lett*. doi:[10.1021/acs.nanolett.5b00440](https://doi.org/10.1021/acs.nanolett.5b00440)
38. Kim JA, Hwang T, Dugasani SR, Amin R, Kulkarni A, Park SH, Kim T (2013) Graphene based fiber optic surface plasmon resonance for bio-chemical sensor applications. *Sensor Actuat B- Chem* 187:426–433. doi:[10.1016/j.snb.2013.01.040](https://doi.org/10.1016/j.snb.2013.01.040)
39. Maharana PK, Srivastava T, Jha R (2014) On the performance of highly sensitive and accurate graphene-on-aluminum and silicon-based SPR biosensor for visible and near infrared. *Plasmonics* 9(5): 1113–1120. doi:[10.1007/s11468-014-9721-4](https://doi.org/10.1007/s11468-014-9721-4)
40. Palik ED, Ghosh G (1985) *Handbook of optical constants of solids*. Academic Press, New York
41. Gan CH, Chu HS, Li EP (2012) Synthesis of highly confined surface plasmon modes with doped graphene sheets in the midinfrared and terahertz frequencies. *Phys Rev B* 85 12:125431–125439. doi: [10.1103/PhysRevB.85.125431](https://doi.org/10.1103/PhysRevB.85.125431)